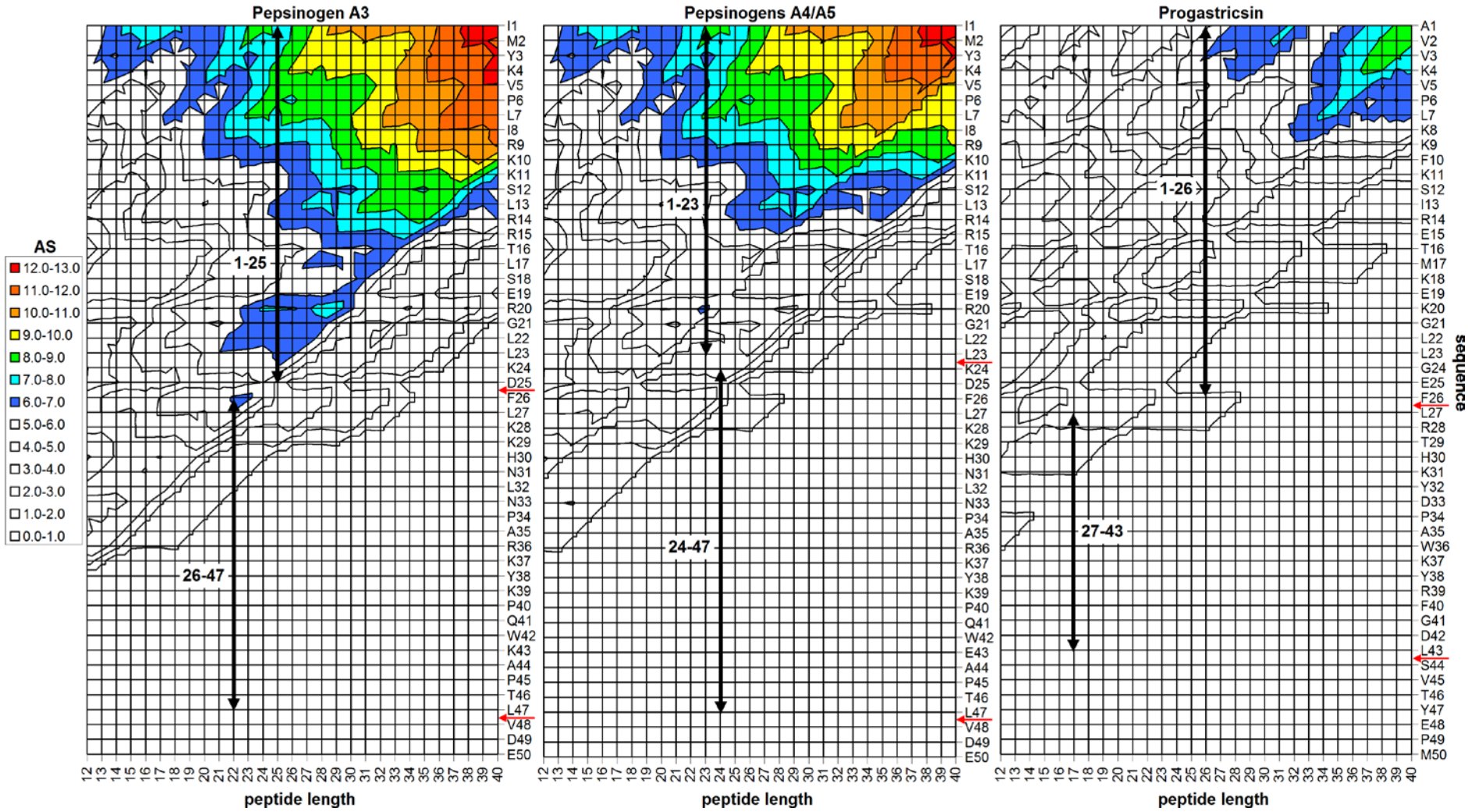

Figure S1. Isometric plots of the absolute scores (AS) of all the peptides of length between 12 and 40 residues in the N-terminus of human pepsinogen A3, pepsinogens A4/A5 and progastricsin. AS values were calculated using the parameters determined for strain *S. aureus* C623 and the hydrophobicity scale Parker-Gly0. Colours highlight scores corresponding to significant hypothetical MIC values, in particular AS > 6 corresponds to a hypothetical MIC lower than 160 µM, AS > 7.6 corresponds to a hypothetical MIC lower than 10 µM. For AS > 9 further increase of the AS values are unlikely to correspond to a decrease of MIC values. Red arrows on the right indicate the major cleavage points in the activation of the zymogen.

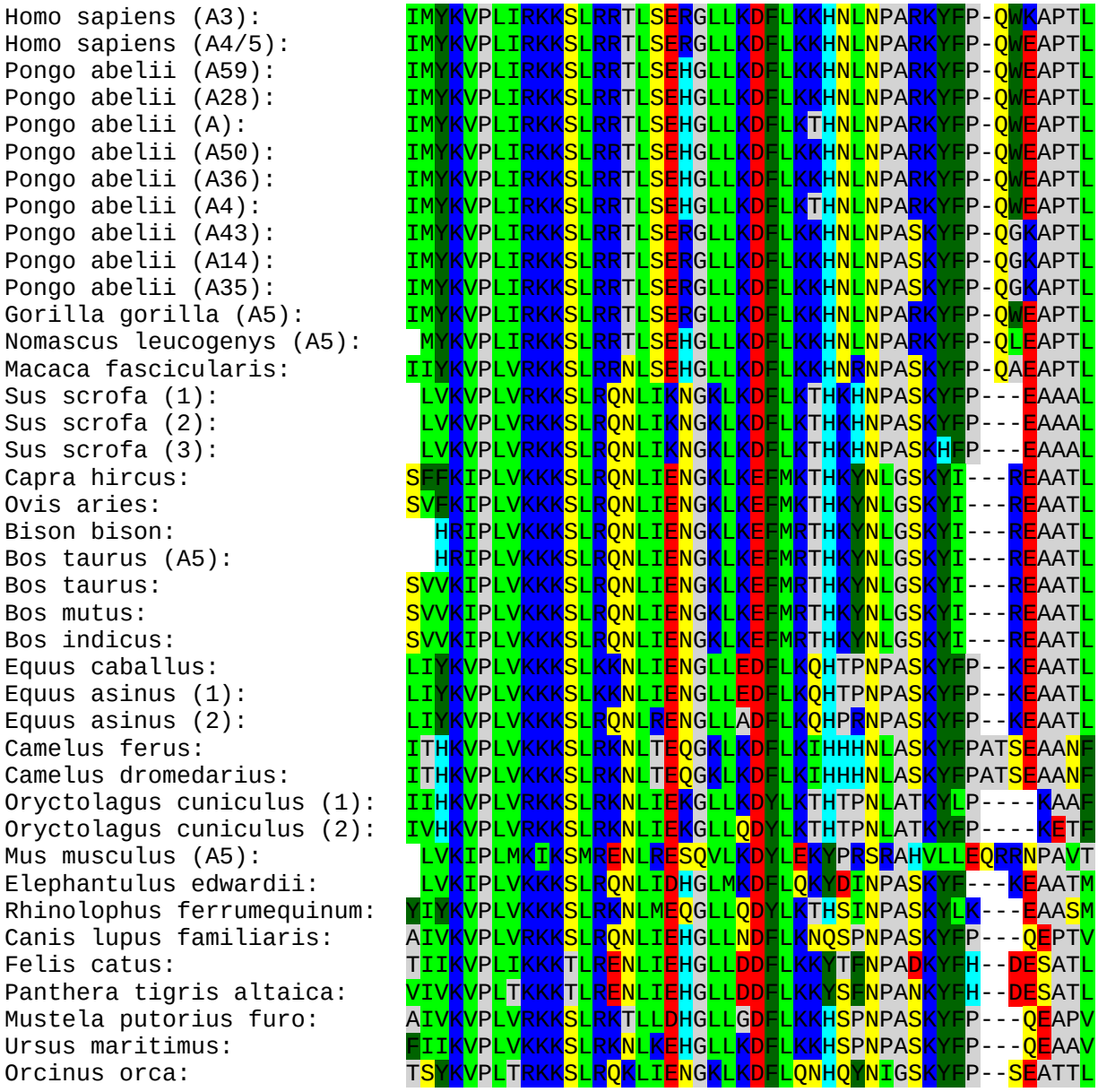

Figure S2. Alignment of the activation peptides of pepsinogen A from several mammals. Residues are colored to show the distribution of charged and hydrophobic residues (blue, basic; red, acidic; yellow, polar uncharged; green, aliphatic/hydrophobic; dark green, aromatic/hydrophobic; gray, borderline; cyan, histidine). The isozymogen name, when defined, is shown in parenthesis, in the other cases the isozymogen were numbered progressively. Sequences are shown in an arbitrary order. The accession numbers of the NCBI protein database are: *Homo sapiens* (A3) "np_001073275.1"; *Homo sapiens* (A4/5) "np_001073276.1"; *Pongo abelii* (A59) "bah20545.1"; *Pongo abelii* (A28) "bah20546.1"; *Pongo abelii* (A) "np_001153272.1"; *Pongo abelii* (A50) "bah20549.1"; *Pongo abelii* (A36) "bah20548.1"; *Pongo abelii* (A4) "xp_002821738.1"; *Pongo abelii* (A43) "bah20539.1"; *Pongo abelii* (A14) "bah20541.1"; *Pongo abelii* (A35) "bah20542.1"; *Gorilla gorilla* (A5) "xp_004051349.1"; *Nomascus leucogenys* (A5) "xp_003282561.1"; *Macaca fascicularis* "xp_005577738.2"; *Sus scrofa* (1) "aaa31096.1"; *Sus scrofa* (2) "aaa31095.1"; *Sus scrofa* (3) "np_999038.2"; *Capra hircus* "xp_005699798.1"; *Ovis aries* "xp_004019629.1"; *Bison bison* "xp_010831445.1"; *Bos taurus* (A5) "aai49645.1"; *Bos taurus* "np_001001600.2"; *Bos mutus* "elr46308.1"; *Bos indicus* "xp_019810172.1"; *Equus caballus* "xp_001501875.1"; *Equus asinus* (1) "xp_014717259.1"; *Equus asinus* (2) "xp_014722425.1"; *Camelus ferus* "xp_006173231.1"; *Camelus dromedarius* "np_001290505.1"; *Oryctolagus cuniculus* (1) "np_001164550"; *Oryctolagus cuniculus* (2) "np_001164549.1"; *Mus musculus* (A5) "np_067428.2"; *Elephantulus edwardii* "xp_006899903.1"; *Rhinolophus ferrumequinum* "bab11751.1"; *Canis lupus familiaris* "np_001003117.1"; *Felis catus* "xp_003993470.1"; *Panthera tigris altaica* "xp_007092068.1"; *Mustela putorius furo* "xp_004770432.1"; *Ursus maritimus* "xp_008705693.1"; *Orcinus orca* "ref"xp_004264225.1"

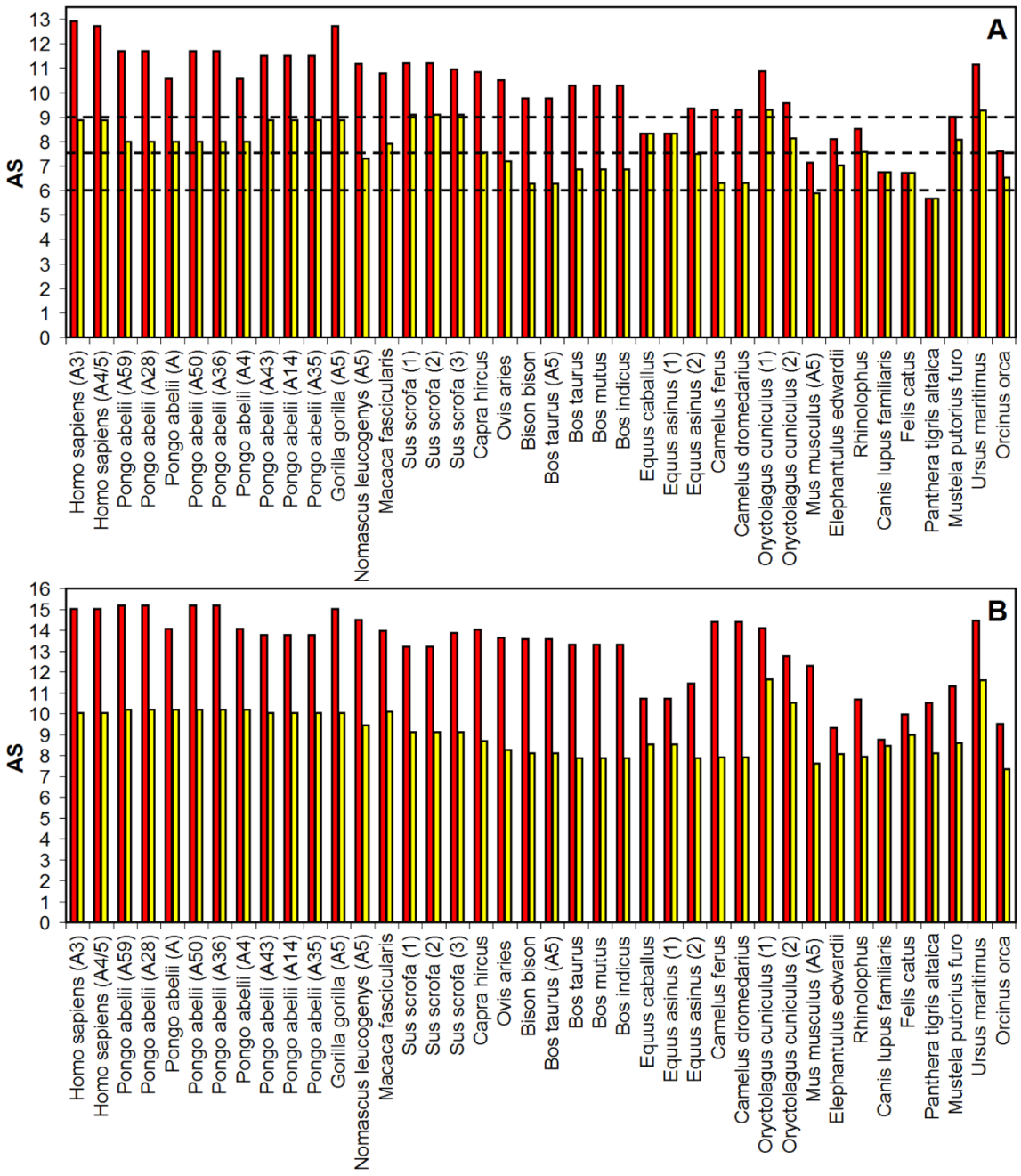

Figure S3. Maximum AS values calculated for peptides longer that 12 residues within the activation peptides of mammalian pepsinogens A shown in Fig. S2. AS values shown as red bars were calculated after analyzing the entire activation peptides and considering as maximal peptide length the length of each activation peptide (from 43 to 48 residues). AS values shown as yellow bars were calculated after analyzing only the N-terminal half of each activation peptide, from residue 1 to the sole completely conserved acidic residue (aspartate 25 in human sequences), and considering as maximal peptide length the length of this N-terminal fragment (from 23 to 25 residues). In panel A, AS values were calculated using the parameters determined for strain *S. aureus* C623, the hydrophobicity scale Parker-Gly0 and the standard protonation states at pH 7.0 (Arg, +1; Lys, +1; Glu, -1; Asp -1). The dashed lines correspond to the three thresholds defined in the legend of Fig. S1. In panel B, AS values were calculated assuming the following protonation states: Arg, +1; Lys, +1; His, +1; Asp -1.

ONC-DCless-H6-(P)PAP-A3

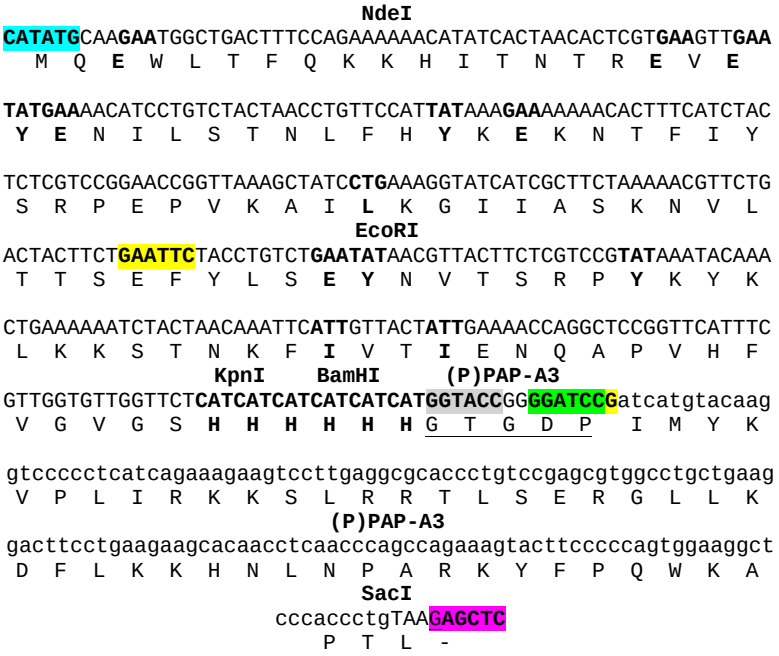

ONC-DCless-H6-(P)PAP-A3(Pro25')

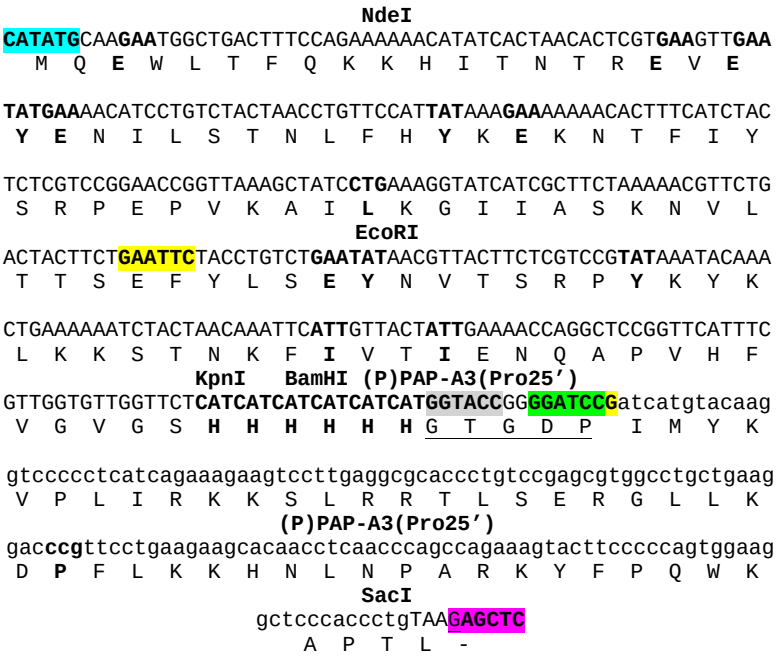

Figure S4. Nucleotide and amino acid sequences. ONC-DCless-H6-(P)PAP-A3 **(upper panel)** and ONC-DCless-H6-(P)PAP-A3(Pro25) **(lower panel)** fusion proteins. Onconase carrier (black); peptide (blue); linker region (red underlined); His_6-Tag (green). Amino acid substitutions in ONC-DCless-H6 carrier sequence, with respect to the Onconase one, are highlighted: glutamic acid residues (red), tyrosine residues (purple), leucine residue (light blue), isoleucine residues (orange). The main restriction enzyme sites were also reported: *NdeI* (turquoise); *EcoRI* (yellow); *KpnI* (grey); *BamHI* (green); *SacI* (pink).

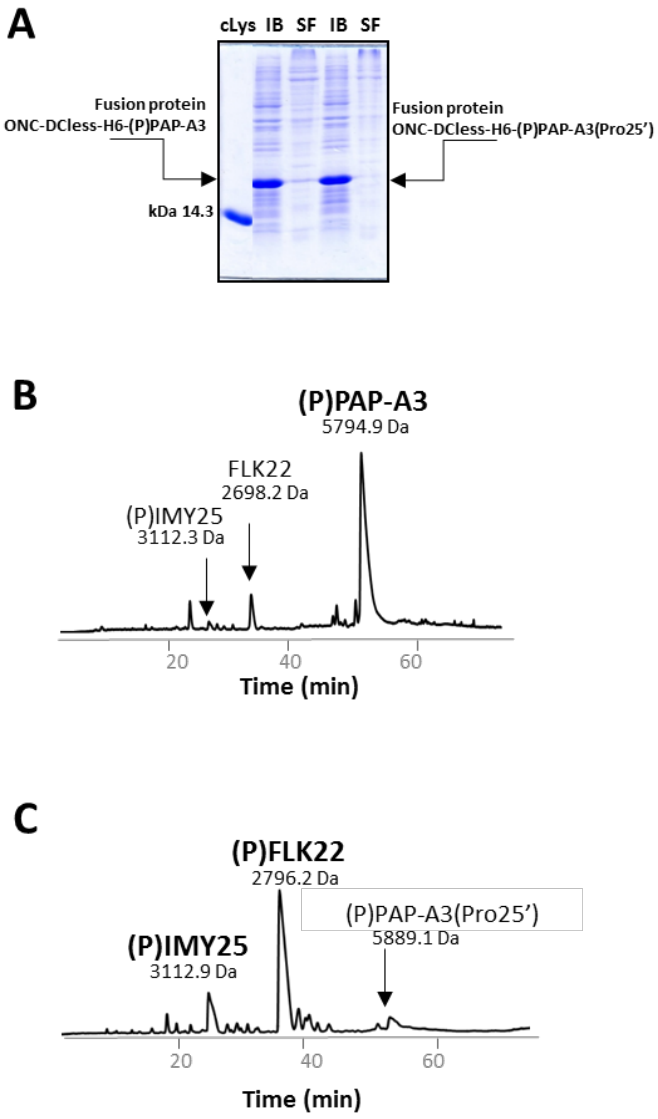

Figure S5. Production of recombinant pepsinogen derived peptides in *E. coli* cells by ONCDCLess-H6 carrier protein A) Expression of recombinant proteins. SDS-PAGE (15%) analysis of the fusion proteins. IB: inclusion bodies after cell lysis; SF: soluble fraction after cell lysis; cLys: *Gallus gallus* lysozyme. **B)** and **C)** RP-HPLC analyses of peptide mixtures derived from acidic cleavage of ONC-DCLess-H6-(P)PAP-A3 (B) and ONC-DCLess-H6-(P)PAP-A3(Pro25') fusion protein (C). Main products derived from each fusion protein are in bold. Molecular weight of peptides, determined by LC-MS, was included in the chromatograms and are also reported in Table S1. Samples were analyzed after selective precipitation of the carrier at neutral pH on Jupiter 5u C18 300Å column.

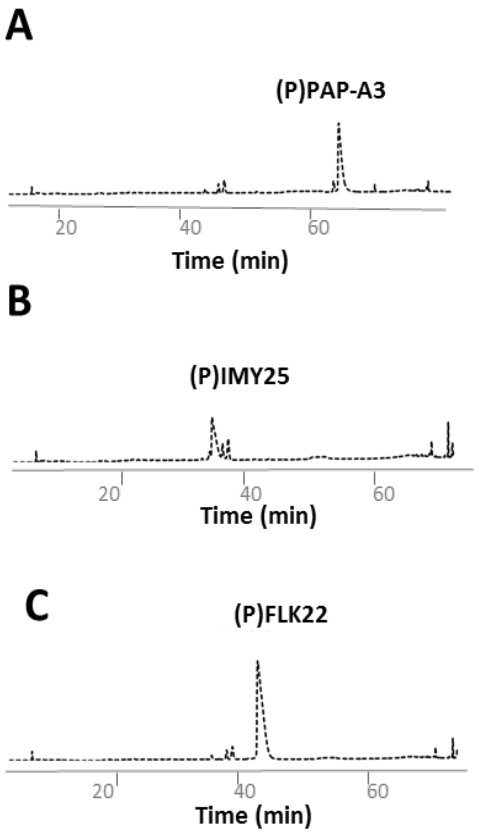

Figure S6. Purity analyses of recombinant peptides. Peptides were analyzed by RP-HPLC on a Jupiter 5u C18 300Å column. **A)** (P)PAP-A3 derived from cleavage of ONC-DCLess-H6-(P)PAP-A3 fusion protein. **B)** and **C)** (P)IMY25 and (P)FLK22 derived from cleavage of ONC-DCLess-H6-(P)PAP-A3(Pro25') respectively.

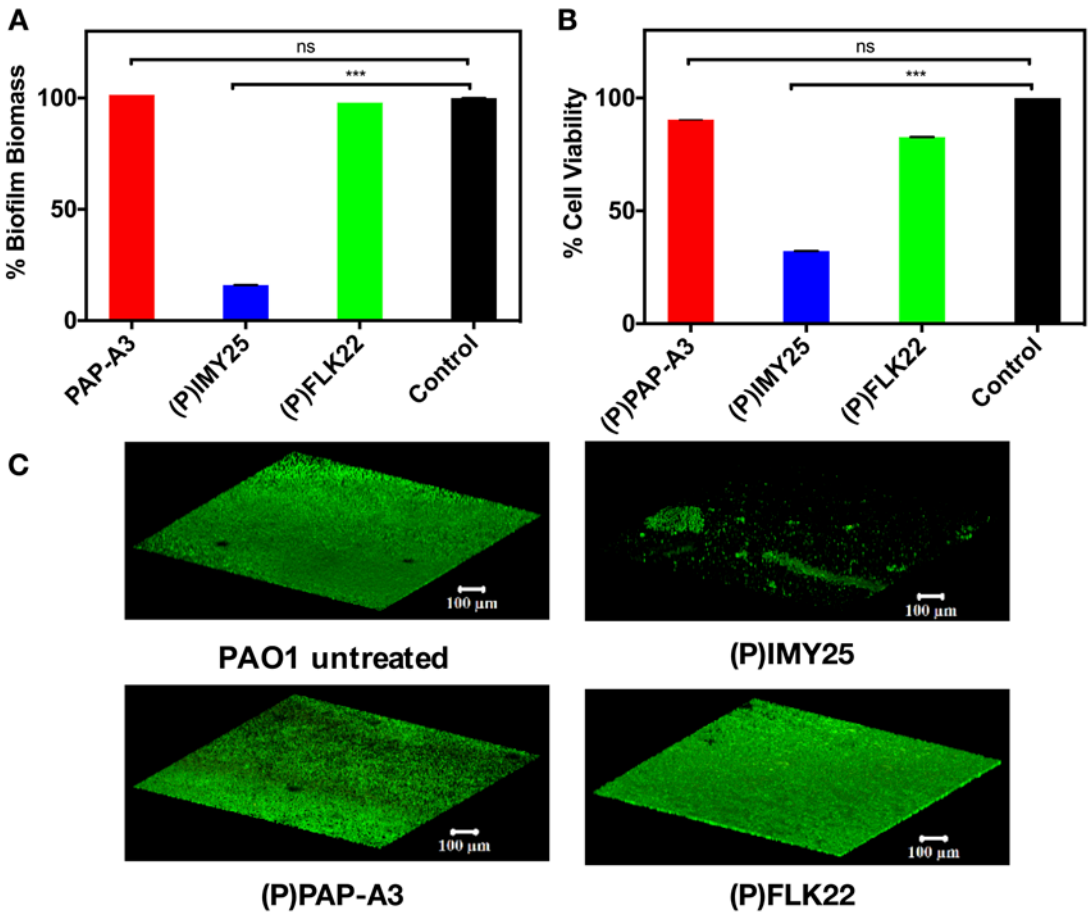

Figure S7. Effect of PAP-A3-derived peptides on *P. aeruginosa* PAO1 preformed biofilm. A) Biofilm biomass was quantified by crystal violet. **B)** Biofilm viability was determined by an XTT reduction assay. Data in percentage are means (± SD) for experiments performed in triplicate. p value of < 0.05 was considered statistically significant. **C)** 3D images (1280 x 1280 mm) obtained by confocal microscopy display the effect of peptides (P)PAP-A3 (top panel), (P)IMY25 (middle panel), and (P)FLK22 (bottom panel) on *P. aeruginosa* PAO1 of one-day-old biofilms treated with 6.25 µM of each peptide compared with *P. aeruginosa* PAO1 untreated samples. All cells stained with SYTO 9 (green) and dead cells stained with PI (red). Scale bars correspond to 100 µm in all cases.

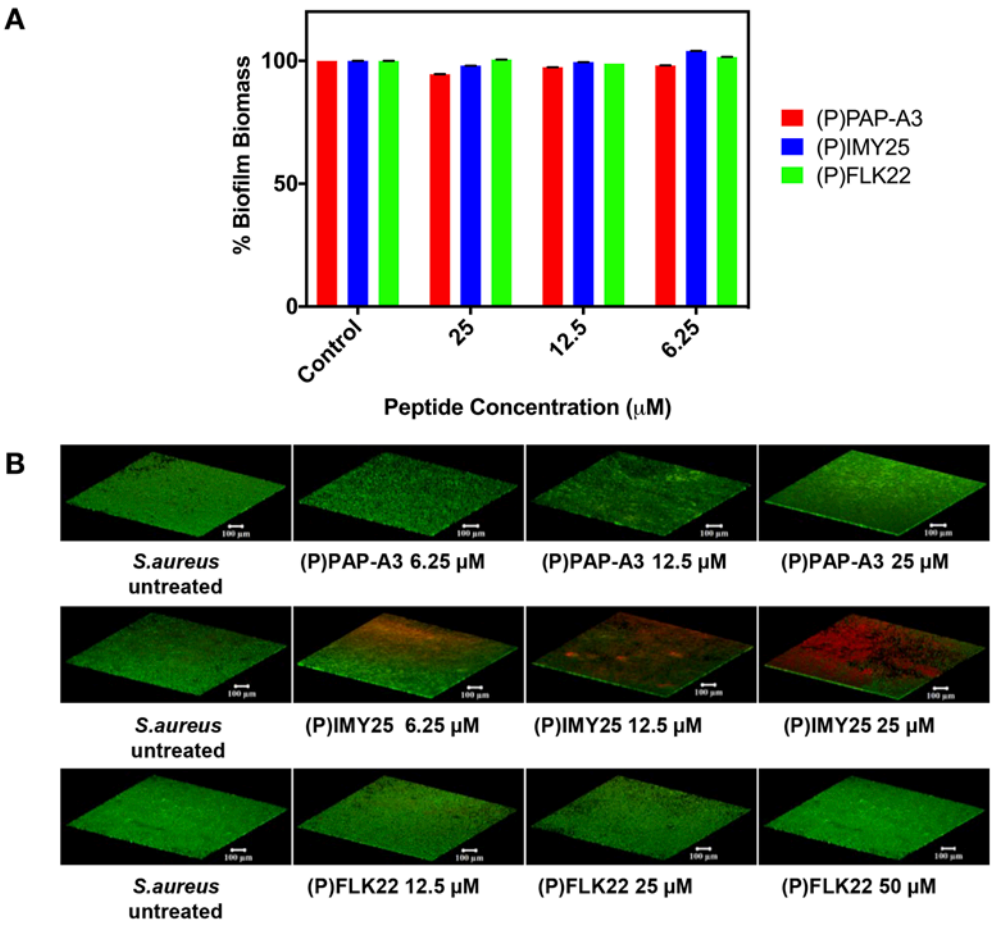

Figure S8. **Effects of different concentrations of PAP-A3, (P)IMY25 and (P)FLK22 on *S. aureus* ATCC6538P mature biofilm. A)** Biofilm biomass was quantified through crystal violet assay. Bars represent the mean (± SD). p value of < 0.05 was considered statistically significant. **B)** 3D images (1280x1280 mm) of *S. aureus* ATCC 6538P displayed the effect of peptides (P)PAP-A3 (top panel), (P)IMY25 (middle panel) and (P)FLK22 (bottom panel) on *S. aureus* one-day-old biofilms treated with different peptide concentrations compared with untreated samples. All cells stained with SYTO 9 (green) and dead cells stained with PI (red). Scale bars correspond to 100 μm in all cases.

Supplemental Results

Differential alginate binding between PAP-A3 and its fragments.

To evaluate the ability of pepsinogen A-derived peptides to bind to alginate, we determined the CD spectra of fixed concentrations of the three peptides (25 µM in the case of (P)PAP-A3 and 50 µM in the case of its fragments) in the presence of increasing concentrations of alginate (Fig. S9A-C). Alginate induced a noteworthy change in the spectra, causing the appearance of a negative peak in the range 196-202 nm, usually associated with random coil conformation and/or a type II polyproline helix, whose CD spectra are very similar and not easily distinguishable [1,2]. The deconvolution of the spectra (Table S2) confirmed that alginate induced unfolding of the three peptides from conformations rich in β-structure to random coil. Such behavior, to the best of our knowledge, has not been reported before.

Even more interestingly, there were significant differences among the three peptides as evidenced by the plot showing molar ellipticity per residue ($\Delta\varepsilon$, M^{-1} cm^{-1}) at 196 nm, as a function of alginate concentration (Fig. S9D). In the case of (P)PAP-A3 and (P)FLK22, absolute $\Delta\varepsilon_{196nm}$ values were very high, -7.5 and -9.95 M^{-1} cm^{-1}, respectively, if compared to the $\Delta\varepsilon_{196nm}$ values expected for a fully disordered random coil and a fully ordered polyproline helix i.e. about -2.3 and -11 M^{-1} cm^{-1}, respectively [1,2]. From these values, it can be roughly estimated that the polyproline helix content of (P)PAP-A3 and (P)FLK22 are about 60% and 88%, respectively. Moreover, the curve for (P)FLK22 showed a pronounced sigmoidal shape, suggesting the existence of a cooperative interaction not observed in the case of (P)PAP-A3. The $\Delta\varepsilon_{196nm}$ values found for (P)IMY25 were considerably lower than those of the two other peptides, suggesting either a weaker binding to the polysaccharide or a lack of significant structural change upon binding. The reduced binding to alginate of (P)IMY25 compared to (P)PAP-A3 and (P)FLK22 may help explain its increased anti-biofilm activity (Figs. S7 and S8).

The differences in the amino acid composition of (P)IMY25 and (P)FLK22 could explain their different behaviors in the presence of alginate. In particular, (P)FLK22 is richer in aromatic residues and prolines (Fig. S2). Moreover, prolines are regularly spaced in the peptide, thus making it unlikely that an α-helical conformation would be adopted, even if this is a secondary structure frequently found in AMPs after their interaction with membranes or alginate [3–5].

Modelling of peptide/alginate complexes

In order to obtain a deeper understanding of the interaction between (P)IMY25, (P)FLK22 and alginate, we modelled the peptides in the presence of short homo-oligomers (26 residues long) of

β-D-mannuronate (M_{26}). The lowest energy structures were determined by a Monte Carlo-based strategy, which has proved useful for the modelling of several biological complexes of different nature and size [6–11].

In agreement with the CD data (Table S2) both peptides showed the ability to fold into alternative structures rich in turns, but while all (P)FLK22 structures (5 different conformations with energy values within 2 kcal/mol) showed compact well packed hydrophobic cores formed in particular by the aromatic residues (Fig. S10), (P)IMY25 structures (only two different conformations with energy values within 1.5 kcal/mol) were less compact with a lower number of hydrophobic contacts and a higher number of ionic/polar interactions made possible by the presence of the two acidic residues (Fig. S11). The existence of alternative structures is not surprising as it is unlikely that peptides of 20-25 residues can adopt a single well-defined folding.

In the models of the alginate complexes, in agreement with the CD data, both peptides adopted unfolded conformations to make multiple contacts with the polysaccharide (Figs. S12, S13 and S14). However, again (P)FLK22 and (P)IMY25 show subtle but interesting differences.

In the case of (P)FLK22 we found several alternative peptide/M_{26} complexes with ΔG values lower than 2 kcal/mol (Fig. S12). These complexes were characterized by stretches of residues in a polyproline helix-like conformation and were stabilized by several (usually 3-5) tight ionic pairs between alginate carboxylate groups and the side chains of arginine and lysine or the positively charged N-terminus. In addition, some complexes (Fig. S12) showed van der Waals/stacking interactions between sugar residues and aromatic side chains whose ability to interact with sugars is well known [12]. In some complexes the peptide wrapped around the oligosaccharide, but we also observed complexes with M_{26} bend on the polypeptide. This finding agrees with the known flexibility of mannuronate-rich polymers [13]. We also noticed that in several complexes only residues 1-5 and 12-19 (containing all the positively charged and aromatic groups) interacted tightly with the oligosaccharide while residues 6-11 behaved as a flexible linker (Fig. S12). Therefore, we tried to model a complex with the peptide spanning between two M_{26} molecules (Fig. S13). The models suggest that residues 1-5 and 12-19 may behave as independent alginate-binding modules. Therefore, at least at high alginate concentrations, the peptide could be constrained to adopt a more extended conformation spanning different molecules of alginate. In this way more alginate molecules could act jointly to promote peptide unfolding, which would be in keeping with the cooperativity evidence shown by the CD data.

In the case of (P)IMY25 we found no additional peptide/M_{26} complex with ΔG values lower than 3 kcal/mol with respect to the most stable one (Fig. S14). The structure of the peptide in this complex showed a less extended structure than those found in the case (P)FLK22 with two turns

allowing the peptide to wrap around the polysaccharide. Moreover, in this complex (P)IMY25 was bound to alginate only through ionic interactions (Fig. S14).

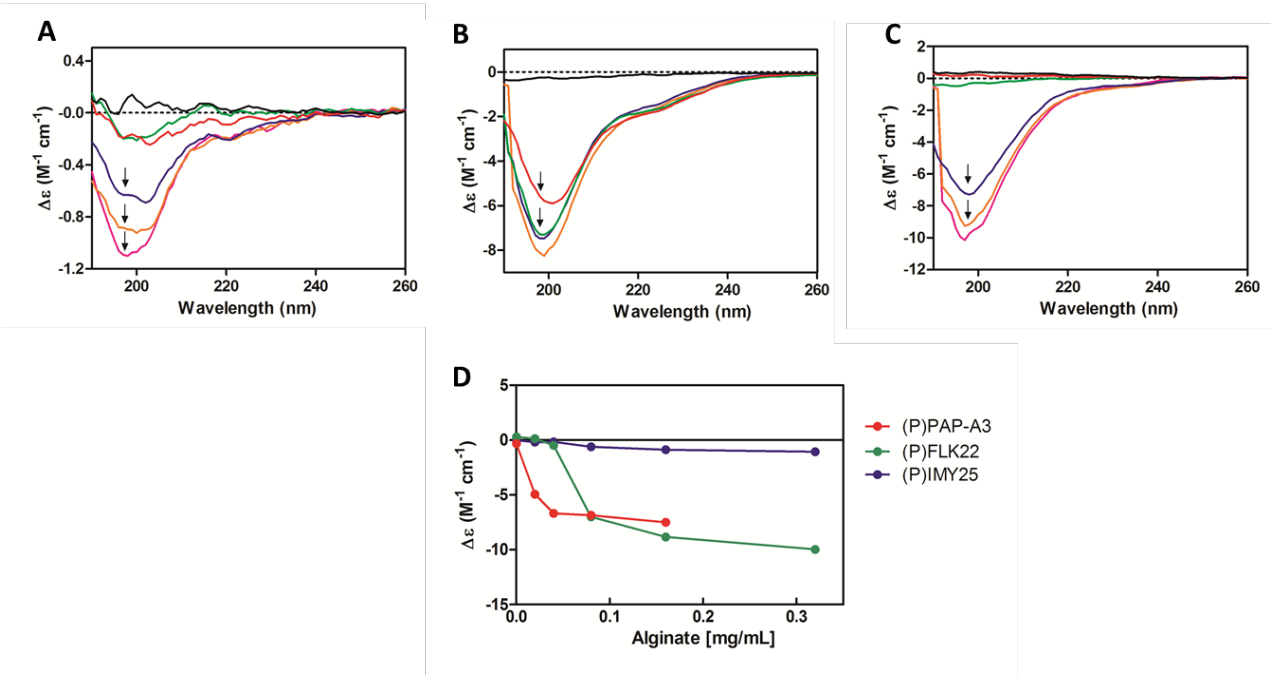

Figure S9. Interaction of cryptic peptides with alginate. A), **B)** and **C)** CD spectra of (P)IMY25, (P)FLK22, and (P)PAP-A3, respectively in the presence of increasing concentrations of alginate. Spectra of peptides in 10 mM buffer phosphate are in black. Red, green, purple, orange and magenta spectra correspond to 0.02 mg/mL, 0.04 mg/mL, 0.08 mg/mL, 0.16 mg/mL and 0.32 mg/mL alginate, respectively. **D)** Plot of the molar absorption per residue ($\Delta\varepsilon$, M^{-1} cm^{-1}) at 196 nm of (P)IMY25 (green), (P)FLK22 (red) and (P)PAP-A3 (black) as a function of alginate concentration.

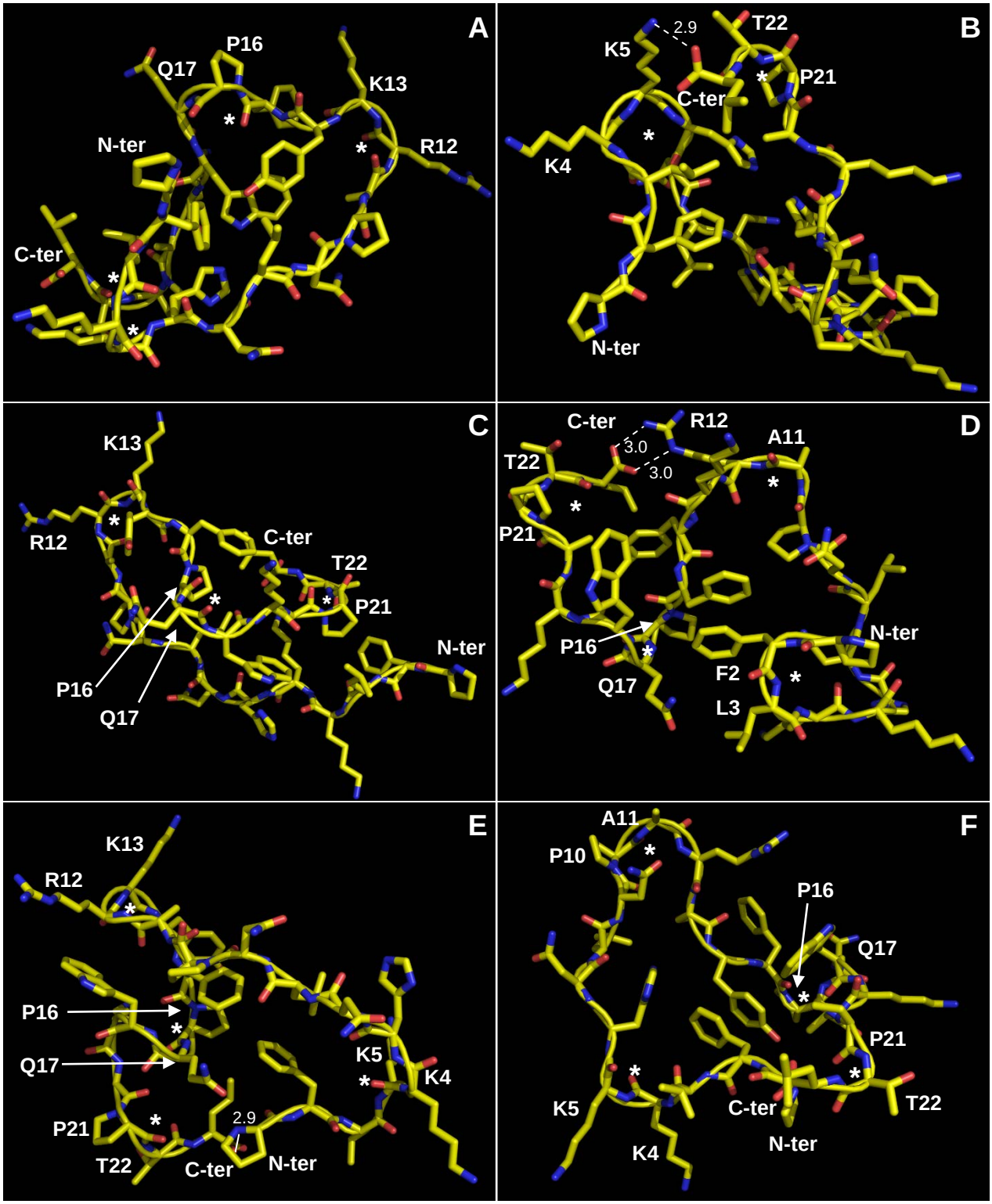

Figure S10. Monte Carlo minimized structures of (P)FLK22. Panels **A)** and **B)** show the lowest energy structure. In panel B) the structure has been rotated with respect to panel A to show more clearly turns K4-K5 and P21-T22. Panels **C-F)** show structures with energy up to 2.5 kcal/mol higher than the lowest energy structure (in order of increasing energy from C to F). Peptide is shown as sticks and cartoon to highlight the backbone path. Atoms are colored according to type (carbon, yellow; nitrogen, blue; oxygen, red). Turns are indicated by asterisks and the corresponding residues are labeled. Ionic pairs with hydrogen bonds are indicated as dotted lines (the corresponding distances are shown in Å).

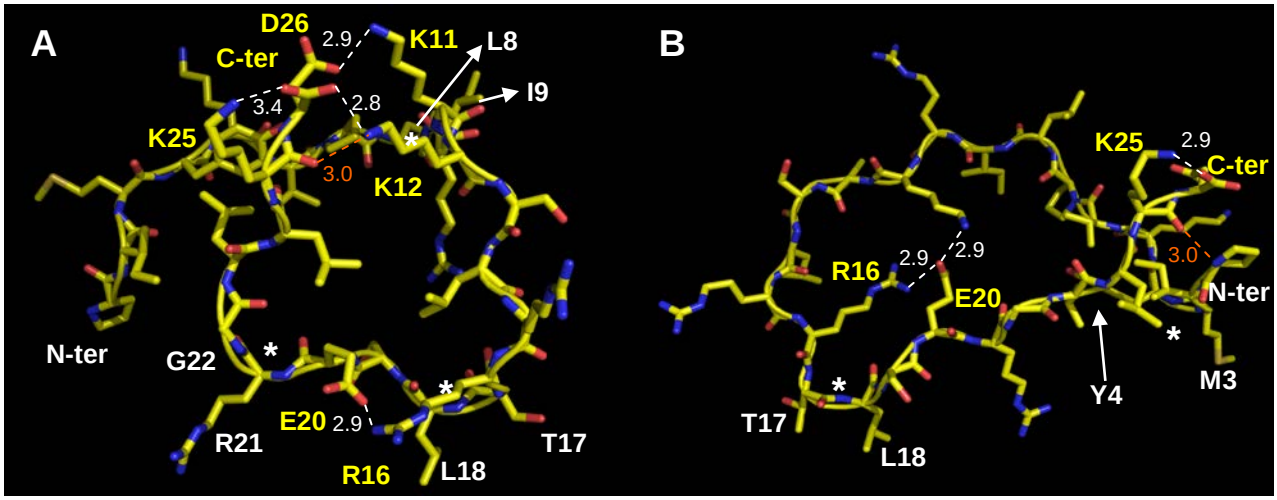

Figure S11. Monte Carlo minimized structures of (P)IMY25. Panel **A)** and **B)** show the lowest energy structure and a structure with energy 1.4 kcal/mol higher than the lowest energy one, respectively. Peptide is shown as sticks and cartoon to highlight the backbone path. Atoms are colored according to type (carbon, yellow; nitrogen, blue; oxygen, red). Turns are indicated by asterisks and the corresponding residues are labeled in white. Ionic pairs with hydrogen bonds are indicated as dotted lines (the corresponding distances are shown in Å) and labeled in yellow. Other H-bonds are in orange.

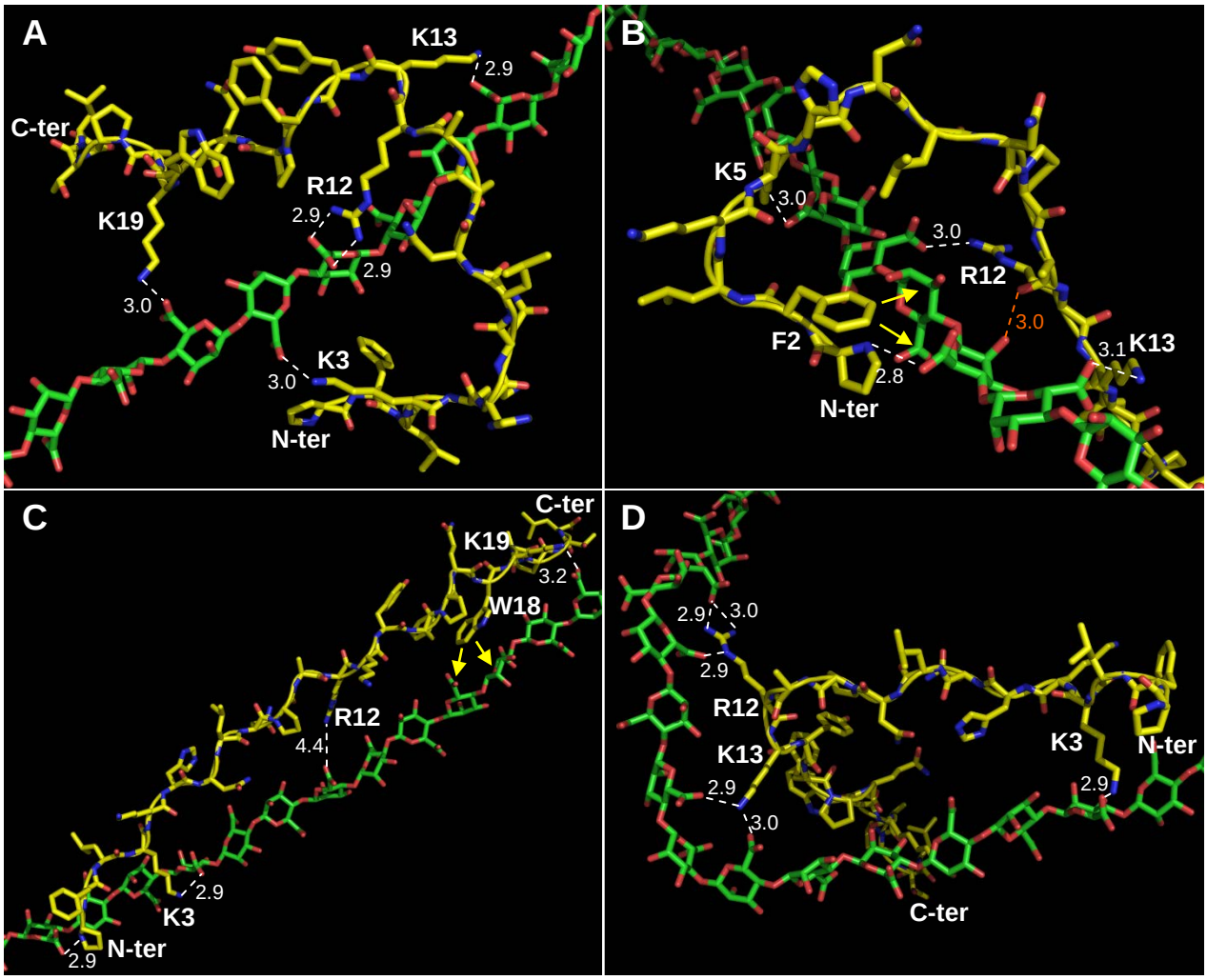

Figure S12. Monte Carlo minimized structures of the complexes of (P)FLK22 with M_{26}. Panel **A)** shows the lowest energy structure for the complex (P)FLK22/M_{26} whereas panels **B-D)** show structures with energy up to 2.8 kcal/mol higher than the lowest energy structure (in order of increasing energy from B to D). Peptide is shown as sticks and cartoon to highlight the backbone path. Atoms are colored according to type (nitrogen, blue; oxygen, red; peptide carbon, yellow; alginate carbon, green). Ionic pairs with hydrogen bonds are indicated as dotted lines (the corresponding distances are shown in Å). Other H-bonds are in orange. Yellow arrows indicate van der Waals contacts between alginate and aromatic residues.

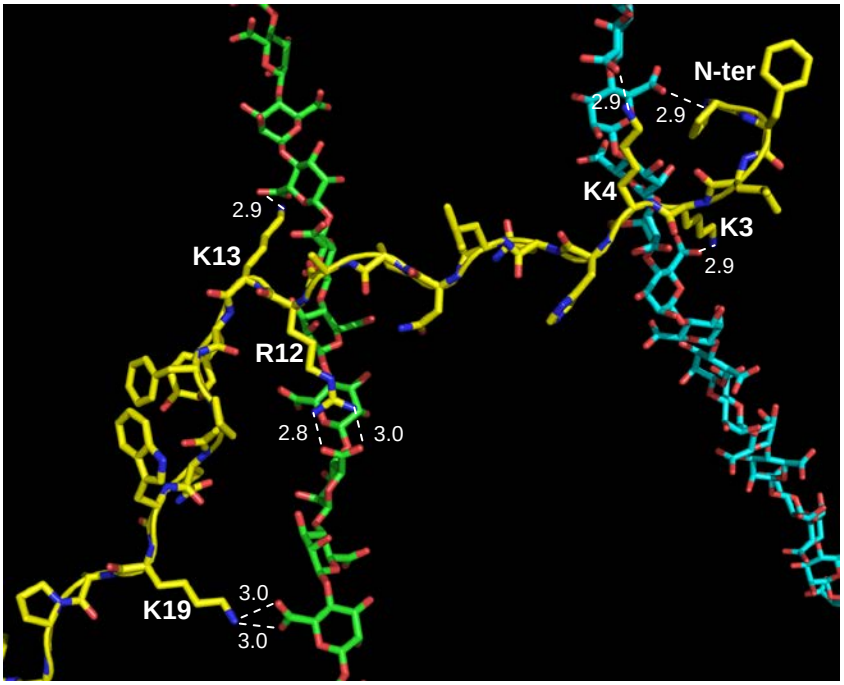

Figure S13. Monte Carlo minimized structures of the complexes of (P)FLK22/$(M_{26})_2$. Peptide is shown as sticks and cartoon to highlight the backbone path. Atoms are colored according to type (nitrogen, blue; oxygen, red; peptide carbon, yellow; alginate carbon, green and cyan for the two M26 molecules). Ionic pairs with hydrogen bonds are indicated as dotted lines (the corresponding distances are shown in Å).

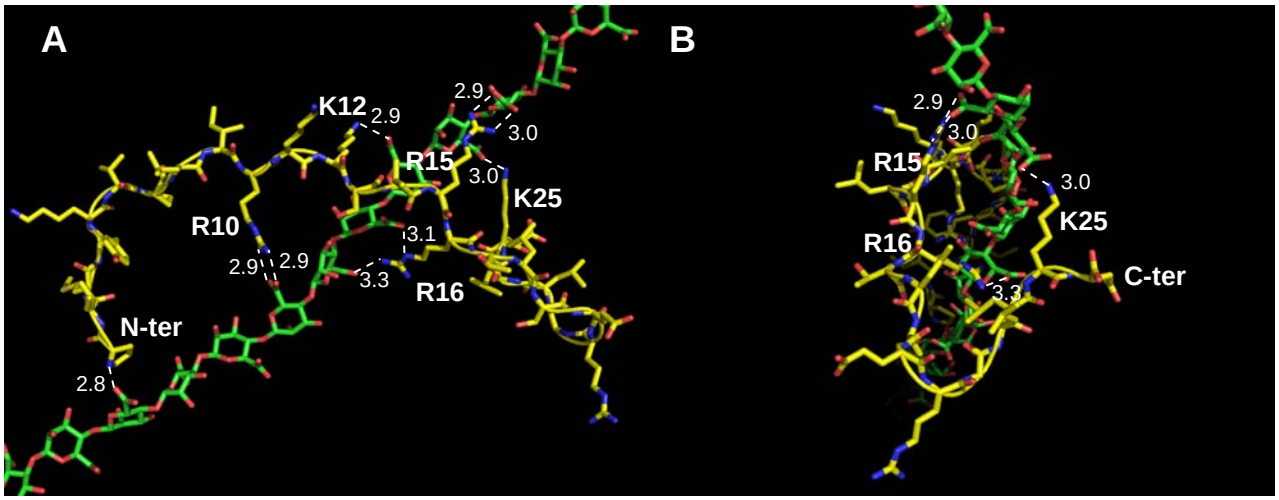

Figure S14. Monte Carlo minimized structure of the complex (P)IMY25/M_{26}. In Panel **B** the structure is rotated clockwise by 90° around the vertical axis with respect to panel **A**. Peptide is shown as sticks and cartoon to highlight the backbone path. Atoms are colored according to type (nitrogen, blue; oxygen, red; peptide carbon, yellow; alginate carbon, green). Ionic pairs with hydrogen bonds are indicated as dotted lines (the corresponding distances are shown in Å).

Table S1. Molecular weight of recombinant pepsinogen derived peptides.

Peptide	Theoretical MW (Da)	Experimental MW (Da)
(P)PAP-A3[a]	5792.0	5794.91
(P)IMY25[a]	3111.8	3112.32
FLK22[a]	2698.21	2698.29
(P)IMY25[b]	3111.8	3112.89
(P)FLK22[b]	2795.3	2796.22

[a] Peptides derived from acidic cleavage of fusion protein ONC-DCLess-H6-(P)PAP-A3

[b] Peptides derived from acidic cleavage of fusion protein ONC-DCLess-H6-(P)PAP-A3(Pro25')

Table S2. Deconvolution of dichroic spectra of (P)IMY25, (P)FLK22 and (P)PAP-A3.

	% α-helix	% β-strand	% Turns[a]	% Coil
(P)IMY25	2.8	49	22.9	25.2
+ Alginate 0.02 mg/ml	0	10.9	28.4	60.8
+ Alginate 0.04 mg/ml	2.8	49	22.9	25.2
+ Alginate 0.08 mg/ml	10.8	34.2	20.8	34.2
+ Alginate 0.16 mg/ml	4	4	2	90
+ Alginate 0.32 mg/ml	4	4	2	90

	% α-helix	% β-strand	% Turns[a]	% Coil
(**P)FLK22**	2.8	49	22.9	25.2
+ Alginate 0.02 mg/ml	2.8	49	22.9	25.2
+ Alginate 0.04 mg/ml	0	10.9	28.4	60.8
+ Alginate 0.08 mg/ml	4	4	2	90
+ Alginate 0.16 mg/ml	4	4	2	90
+ Alginate 0.32 mg/ml	4	4	2	90

	% α-helix	% β-strand	% Turns[a]	% Coil
(**P)PAP-A3**	2.8	49	22.9	25.2
+ Alginate 0.02 mg/ml	4	4	2	90
+ Alginate 0.04 mg/ml	4	4	2	90
+ Alginate 0.08 mg/ml	4	4	2	90
+ Alginate 0.16 mg/ml	4	4	2	90

[a] Deconvolution was obtained by DICHROWEB tool using algorithm Selcon 3 and the reference dataset 7.

Supplemental Experimental Procedures

Recombinant vectors

ONC-DCless-H6-(P)PAP-A3 and ONC-DCless-H6-(P)PAP-A3(Pro26) fusion proteins were produced by using *pET22b(+)/ONC-DCless-H6-(P)PAP-A3* and *pET22b(+)/ONC-DCless-H6-(P)PAP-A3(Pro26)* recombinant plasmids, respectively (Fig. S4). DNA sequence coding for the fusion proteins were obtained by chemical synthesis (MWG-Biotech AG; Ebersberg, Germany). *NdeI* and *SacI* restriction sites (New England Biolabs, Ipswich, MA, USA) were introduced at 5'- and 3'-end of the synthetic genes, respectively, for their cloning into pET22b(+) vector (Novagen, San Diego, CA, USA). *E. coli* strain TOP10F' (Invitrogen, San Diego, CA, USA) was used for cloning procedures according to Sambrook [14]. Wizard SV Gel, PCR Clean-Up DNA Purification System and T4 DNA ligase were obtained from Promega (Madison, WI, USA). QIAprep spin miniprep (Germantown, MD, USA). DNA sequencing were performed from MWG-Biotech AG (Ebersberg, Germany). ONC-DCless-H6-(P)GKY20 fusion protein was expressed by *pET22b(+)/ONC-DCless-H6-(P)GKY20* plasmid.

Protein expression and purification of recombinant peptides

Recombinant proteins were expressed in *Escherichia coli* BL21(DE3) (Novagen, San Diego, CA, USA), as previously described for ONC-DCless-H6-(P)GKY20 fusion protein [15]. Briefly, bacterial cultures grown in TB medium supplemented with 0.4% glucose and 100 µg/mL ampicillin at 37°C, were induced at mid-log phase with 0.4 mM IPTG. After overnight induction at 37°C under shaking, cells were harvested by centrifugation at 8000x g for 15 min at 4°C. The bacterial pellets were suspended in 50 mM Tris-HCl, pH 7.4, containing 10 mM EDTA, and sonicated in a cell disruptor (10 x 1 min cycle, on ice). The suspensions were then centrifuged at 18,000 x g for 60 min at 4°C. Soluble and insoluble fractions were analyzed by SDS-PAGE [16].

The insoluble fractions containing recombinant proteins as inclusion bodies, were washed three times in 0.1 M Tris-HCl, pH 7.4, containing 10 mM EDTA, 2% Triton X-100 and 2 M urea, followed by repeated washes in 0.1 M Tris-HCl, pH 7.4, to eliminate residual traces of Triton, urea and EDTA. Recombinant proteins were purified by immobilized metal ion affinity chromatography (IMAC), using the Ni Sepharose™ 6 Fast Flow resin (GE Healthcare, Uppsala, Sweden) in denaturing conditions. Routinely, 100 mg of fusion proteins were dissolved in 10 mL of binding buffer (6 M guanidine/HCl in 50 mM Tris-HCl, pH 7.4). Purified protein concentrations were determined by spectrophotometric analyses using the extinction coefficients calculated by the ProtParam tool (http://web.expasy.org/protparam/) [17] [ONC-DCless-H6-(P)PAP-A3 and ONC-DCless-H6-(P)PAP-A3(Pro25') proteins: ε_{280} = 24,410 M^{-1} cm^{-1}, ε_{280} (0.1%) = 1.28; ONC-DCless-

H6-(P)GKY20 protein: ε_{280} = 24,410 M^{-1} cm^{-1}; ε_{280} (0.1%) = 1.53)]. Purified proteins were extensively dialyzed against 0.1 M acetic acid at 4°C, at pH 3. The release of peptides from fusion proteins was performed in mild acid conditions (incubation for 24 h at 60°C in 0.1 M acetic acid, 18 mM HCl, pH 2.0, under nitrogen atmosphere). Cleavage efficiency of Asp-Pro sequences into the linker region was determined by densitometric analysis of 20% SDS-PAGE (ChemiDoc detection system, Bio-Rad; Quantity One software). Formaldehyde 4% in Coomassie Blue staining solution (0.2% Coomassie Brilliant Blue R-250, 25% isopropyl alcohol and 10% glacial acetic acid) was used to covalently link proteins and polypeptides in polyacrylamide gels [18]. In order to separate carrier protein from peptides, the pH of the mixtures was adjusted to 7.0–7.2 (with NH_3), and soluble peptides were isolated from the insoluble carrier through repeated cycles of centrifugation.

Purified pepsinogen derived peptides were analyzed by SDS-PAGE (20%) and reverse-phase high performance liquid chromatography (RP-HPLC) carried out with a Jasco LC-4000 system equipped with PU-4086 semipreparative pumps and MD-4010 photo diode array detector.

The column (Jupiter 5u C18 300A column 250 x 4,6 mm, 5 µm particle size, Phenomenex, California, USA) was equilibrated with 5% acetonitrile (0.05% TFA) and peptides were eluted by the following gradient: isocratic elution at 5% solvent B for 10 min, from 5% to 20% solvent B in 5 min, from 20% to 30% solvent B in 40 min, from 30% to 40% solvent B in 5 min, from 40% to 95% solvent B in 5 min. The elution was monitored at 280 nm at a flow rate of 1 ml/min. Degree of fragmentation at internal cleavage sites of peptide mixtures after precipitation at neutral pH, was calculated by normalization of the RP-HPLC peak areas with extinction coefficient calculated by the PlotParam tool (listed below). The identity of peptides was assessed by Mass spectrometry analyses.

Pepsinogen derived peptides were further purified by RP-HPLC. The column (Europa Protein 300 C18 5 µm, 25 x 1, Teknokroma, Barcelona, Spain) was equilibrated in 5% acetonitrile (0.05% TFA) and peptides were loaded in 5% acetonitrile (0.1% TFA) at flow rate of 2 mL/min. Peptides were eluted by the following gradient: isocratic elution at 5% solvent B for 10 min, from 5% to 20% solvent B in 5 min, from 20% to 30% solvent B in 85 min, from 30% to 95% solvent B in 1 min. The elution was monitored at 280 nm at a flow rate of 2 mL/min.

Purified peptide concentrations were determined by spectrophotometric analysis using the extinction coefficients calculated by the ProtParam tool [17]. [(P)PAP-A3: ε_{280} = 8,480 M^{-1} cm^{-1}; ε_{280} (0.1%) = 1.46; (P)IMY25: ε_{280} = 1,490 M^{-1} cm^{-1}; ε_{280} (0.1%) = 0.48; FLK22: ε_{280} = 6,990 M^{-1} cm^{-1}; ε_{280} (0.1%) = 2.59; (P)PAP-A3(Pro26): ε_{280} = 8,480 M^{-1} cm^{-1}; ε_{280} (0.1%) = 1.44; (P)FLK22: ε_{280} = 6,990 M^{-1} cm^{-1}; ε_{280} (0.1%) = 2.50)]. Purity of peptides was assessed by RP-HPLC on Jupiter 5u

C18 300Å column (250 x 4.6 mm, 5µm particle size) as described above. Peptide identity was determined by Mass spectrometry. Purified peptides were lyophilized and stored at -80 °C.

Mass Spectrometry

Mass analyses were performed on MALDI-TOF micro MX spectrometer (Waters, Manchester, UK). 1 µL of digestion mixtures or each peptide solution was mixed with 1 µL of saturated α-cyano-4-hydroxycinnamic acid matrix solution [10 mg/mL in acetonitrile: 0.1% TFA (1:1; v/v)]. Thus, a droplet of the resulting mixture (1 µL) was placed on the mass spectrometer's sample target and dried at room temperature. Once the liquid was completely evaporated, samples were loaded into the mass spectrometer and analysed. The instrument was externally calibrated using a tryptic alcohol dehydrogenase digest (Waters, Manchester, UK) in reflectron mode. For linear mode, a four-point external calibration was applied using an appropriate mixture (10 pmol/mL) of insulin, cytochrome C, horse Mb and trypsinogen as standard proteins (Sigma). A mass accuracy near to the nominal (50 and 300 ppm in reflectron and linear modes, respectively), was achieved for each standard. All spectra were processed and analysed using MassLynx 4.0 software.

Crystal violet (CV) assays

A fresh culture on trypticase soy agar (TSA) was resuspended at a turbidity of 0.5 McFarland ($1x10^8$ CFU/mL) into nutrient broth (NB) with 0.5% glucose, and then diluted to obtain a suspension concentration of $1x10^5$ CFU/mL. Bacterial cells were seeded into flat-bottom 96-well polypropylene microtiter plate (Eppendorf, Hamburg, Germany) and incubated overnight at 37 °C. After that, planktonic cells were removed and adhering cells were exposed to serially two-fold dilution peptide concentrations (from 25 µM up to 6.25 µM) in NB and furtherly incubated for 24 h at 37 °C. After treatment, planktonic cells were removed, biofilms were stained with 0.5% crystal violet for 15 min. Subsequently dye was removed and after rinsing each well with PBS, 99% ethanol was added to each well and incubated for 20 min at room temperature. Then, the OD_{595} was measured.

XTT assays

The metabolic activity of cells after peptides treatment was carried out by XTT assay (Roche Diagnostics Corporation, Indianapolis, IN, USA). Planktonic cells were removed and the wells were washed twice with PBS. Then 200 µl of XTT was added to each well and the plate incubated in the dark for 40 min at 37 °C. The reduction of the tetrazolium salt into orange formazan dye was measured at 490 nm. The medium was also set as negative control. Viability values were compared for each well with respect to controls.

Circular dichroism

CD measurements were recorded on a Jasco-720 spectropolarimeter over the wavelength interval of 190-260 nm, at 20 °C using a 0.1 cm optical path length quartz cuvette. Peptides were dissolved in 10 mM sodium phosphate buffer (pH 7.0) at concentrations of 50 µM [(P)IMY25 and (P)FLK22] and 25 µM for (P)PAP-A3. CD spectra were recorded with a time constant of 4 s, a 2 nm bandwidth, and a scan rate of 10 nm min^{-1}. The spectra were signal-averaged over at least three scans and the baseline was corrected by subtracting the complete buffer spectrum. Spectra were recorded in the presence of increasing concentrations of seaweed alginate (Sigma Aldrich): 0.02-0.04-0.08-0.16-0.32 mg/mL. In this case, the baseline was corrected by subtracting the spectrum of alginate alone at the same concentration tested. Spectra were not collected at concentrations higher than 0.16 mg/mL, in the case of (P)PAP-A3, and of 0.32 mg/mL, in the case of (P)IMY25 and (P)FLK22, because of the rapid appearance of macroscopic aggregates.

Molecular docking

All calculations were performed using the ZMM-MVM molecular modelling package (ZMM Software Inc. [http://www.zmmsoft.com]) essentially as previously described [8]. All energy calculations included a hydration component as previously described [19,20].

(P)FLK22 was modelled with protonated N-terminus and deprotonated C-terminus. Histidine at position 6 was modelled in the neutral form. Two homo-oligosaccharides were modelled containing either 26 β-D-mannuronate or 26 α-L-guluronate residues. Firstly, trisaccharides were prepared and optimized using the AM1 semiempirical method in HyperChem (Hypercube Inc.), hence the trisaccharides were imported in ZMM using the ZL module to prepare the molecular description of the two terminal and internal units. Root atoms for the Monte Carlo sampling were placed at the nitrogen atom of Arg-12 in the case of the peptide and at the C5 atom of residue 13 and C1 atom of residue 14 in the case of the oligosaccharides.

Initial structures of the complexes were prepared using PyMOL (DeLano Scientific LLC, https://www.pymol.org/) and DeepView - Swiss-PdbViewer [21]. For the modelling of the peptide three arbitrary initial models were prepared, a completely α-helical, a completely extended structure and a polyproline-like structure. The three models were then used to generate forty arbitrary starting complexes for each of the two oligosaccharides: each peptide model was placed parallel to the oligosaccharide with the root atom above the central bond of the oligosaccharide, either with the N-terminus toward the reducing end or the toward the non-reducing end, hence the peptide structure was rotated by steps of 90°, in the case of the extended structure, or by steps of 120°, in the case of

the α-helical and the polyproline-like structure. A similar set of twenty structures was prepared placing the peptide model perpendicular to the oligosaccharide.

Each peptide model and manual complex was used as starting point for a Monte Carlo trajectory. Trajectories were stopped after 80,000 cycles or when no energy decrease was observed for 6,000 minimization cycles.

Hemolytic assays

EDTA anti-coagulated mouse blood was centrifuged for 10 min at 800 ×g (20 °C) to sediment the red blood cells (RBCs). Pelleted RBCs were washed three times and diluted 200-fold in PBS. In 96-well polypropylene plates, 75 μL of two-fold serially diluted peptide (from 40 up to 0.31 μM) were mixed with an equal volume of RBC suspension and incubated for 1 h at 37 °C. PBS was used as negative control (blank) whereas 0.2% (v/v) Triton X-100 solution as positive control. Supernatants, collected after 10 min centrifugation at 1300 ×g (20 °C), were transferred into polystyrene 96-wells plates and OD_{405} was measured. Hemolysis (%) was calculated as follows: $[(A_{Peptide} - A_{Blank}) / (A_{Triton} - A_{Blank})] \times 100$.

Supplemental References

(1) Lam, S. L.; Hsu, V. L. NMR Identification of Left-Handed Polyproline Type II Helices. *Biopolymers* **2003**, *69* (2), 270–281.

(2) Ruzza, P.; Calderan, A.; Guiotto, A.; Osler, A.; Borin, G. Tat Cell-Penetrating Peptide Has the Characteristics of a Poly(Proline) II Helix in Aqueous Solution and in SDS Micelles. *J. Pept. Sci.* **2004**, *10* (7), 423–426.

(3) Chan, C.; Burrows, L. L.; Deber, C. M. Helix Induction in Antimicrobial Peptides by Alginate in Biofilms. *J. Biol. Chem.* **2004**, *279* (37), 38749–38754.

(4) Chan, C.; Burrows, L. L.; Deber, C. M. Alginate as an Auxiliary Bacterial Membrane: Binding of Membrane-Active Peptides by Polysaccharides*. *J. Pept. Res.* **2005**, *65* (3), 343–351.

(5) Kuo, H. H.; Chan, C.; Burrows, L. L.; Deber, C. M. Hydrophobic Interactions in Complexes of Antimicrobial Peptides with Bacterial Polysaccharides. *Chem. Biol. Drug Des.* **2007**, *69* (6), 405–412.

(6) Zanfardino, A.; Restaino, O. F.; Notomista, E.; Cimini, D.; Schiraldi, C.; De Rosa, M.; De Felice, M.; Varcamonti, M. Isolation of an Escherichia Coli K4 KfoC Mutant Over-Producing Capsular Chondroitin. *Microb. Cell Fact.* **2010**, *9* (1), 34.

(7) Notomista, E.; Cafaro, V.; Bozza, G.; Di Donato, A. Molecular Determinants of the Regioselectivity of Toluene/o-Xylene Monooxygenase from Pseudomonas Sp. Strain OX1. *Appl. Environ. Microbiol.* **2009**, *75* (3), 823–836.

(8) Siepi, M.; Morales-Narváez, E.; Domingo, N.; Monti, D. M.; Notomista, E.; Merkoçi, A. Production of Biofunctionalized MoS_2 Flakes with Rationally Modified Lysozyme: A Biocompatible 2D Hybrid Material. *2D Mater.* **2017**, *4* (3), 035007.

(9) De Rosa, M.; Zanfardino, A.; Notomista, E.; Wichelhaus, T. A.; Saturnino, C.; Varcamonti, M.; Soriente, A. Novel Promising Linezolid Analogues: Rational Design, Synthesis and

Biological Evaluation. *Eur. J. Med. Chem.* **2013**, *69*, 779–785.
(10) Donadio, G.; Sarcinelli, C.; Pizzo, E.; Notomista, E.; Pezzella, A.; Di Cristo, C.; De Lise, F.; Di Donato, A.; Izzo, V. The Toluene O-Xylene Monooxygenase Enzymatic Activity for the Biosynthesis of Aromatic Antioxidants. *PLoS One* **2015**, *10* (4), e0124427.
(11) Notomista, E.; Scognamiglio, R.; Troncone, L.; Donadio, G.; Pezzella, A.; Di Donato, A.; Izzo, V. Tuning the Specificity of the Recombinant Multicomponent Toluene O-Xylene Monooxygenase from Pseudomonas Sp. Strain OX1 for the Biosynthesis of Tyrosol from 2-Phenylethanol. *Appl. Environ. Microbiol.* **2011**, *77* (15), 5428–5437.
(12) Guillén, D.; Sánchez, S.; Rodríguez-Sanoja, R. Carbohydrate-Binding Domains: Multiplicity of Biological Roles. *Appl. Microbiol. Biotechnol.* **2010**, *85* (5), 1241–1249.
(13) Hecht, H.; Srebnik, S. Structural Characterization of Sodium Alginate and Calcium Alginate. *Biomacromolecules* **2016**, *17* (6), 2160–2167.
(14) Molecular Cloning. *Cold Spring Harb. Lab. Press* **2012**.
(15) Pane, K.; Durante, L.; Pizzo, E.; Varcamonti, M.; Zanfardino, A.; Sgambati, V.; Di Maro, A.; Carpentieri, A.; Izzo, V.; Di Donato, A.; et al. Rational Design of a Carrier Protein for the Production of Recombinant Toxic Peptides in Escherichia Coli. *PLoS One* **2016**, *11* (1), e0146552.
(16) Laemmli, U. K. Cleavage of Structural Proteins during the Assembly of the Head of Bacteriophage T4. *Nature* **1970**, *227* (5259), 680–685.
(17) Gasteiger, E.; Hoogland, C.; Gattiker, A.; Duvaud, S.; Wilkins, M. R.; Appel, R. D.; Bairoch, A. Protein Identification and Analysis Tools on the ExPASy Server. In *The Proteomics Protocols Handbook*; Humana Press: Totowa, NJ, 2005; pp 571–607.
(18) Steck, G.; Leuthard, P.; Bürk, R. R. Detection of Basic Proteins and Low Molecular Weight Peptides in Polyacrylamide Gels by Formaldehyde Fixation. *Anal. Biochem.* **1980**, *107* (1), 21–24.
(19) Weiner, S. J.; Kollman, P. A.; Case, D. A.; Singh, U. C.; Ghio, C.; Alagona, G.; Profeta, S.; Weiner, P. A New Force Field for Molecular Mechanical Simulation of Nucleic Acids and Proteins. *J. Am. Chem. Soc.* **1984**, *106* (3), 765–784.
(20) Lazaridis, T.; Karplus, M. Effective Energy Function for Proteins in Solution. *Proteins* **1999**, *35* (2), 133–152.
(21) Guex, N.; Peitsch, M. C. SWISS-MODEL and the Swiss-PdbViewer: An Environment for Comparative Protein Modeling. *Electrophoresis* **1997**, *18* (15), 2714–2723.